ROYAL SOCIETY
OF CHEMISTRY

Check for updates

Quantum engineering of mixed-valence 1D conjugated polymers

Lesly Katherine Sánchez De La Cruz,[a] Jordi Ribas-Arino, [iD][a] Stefan T. Bromley [iD][ab] and Isaac Alcón [iD] *[a]

One dimensional conjugated polymers (1DCPs) that host periodic arrays of unpaired electrons are gaining increasing attention as atomically-precise correlated materials for future quantum technologies. 1DCPs based on triarylmethyls (TAM) are particularly interesting, due to the persistent nature of TAM radicals and the possibility to control the delocalization of their unpaired electrons *via* different means. However, the known strategies to effectively control the quantum ground-state of these organic systems is still limited. Here, by means of first principles density functional theory (DFT) calculations, we propose the use of a rational periodic substitution of radical sp^2 carbon (C) sites in TAM 1DCPs by sp^2 nitrogen (N) atoms, as a means to tailor the quantum state of the resulting mixed-valence (mv) 1DCP. In particular, we explore a fully alternating N-substitution pattern (NCNC) and a semi-alternating one (NNCC), and show that the former gives rise to a robust multiradical open-shell configuration, whereas the latter leads to a closed-shell quinoidal state. *Via ab initio* molecular dynamics simulations, we demonstrate that such quantum engineering of mv-1DCPs is robust to thermal fluctuations at room temperature, which highlights the technological viability of our approach for future molecular scale quantum electronics and spintronics.

Introduction

During the last two decades bottom-up on-surface synthesis (OSS) has been shown to be a powerful technique to fabricate carbon nanostructures with atomic precision.[1,2] In OSS, rationally designed organic building blocks are deposited on metallic surfaces, where they re-arrange in an ordered fashion. Upon increasing temperature, intermolecular reactions occur between neighbouring molecules, leading to the formation of low-dimensional carbon nanostructures.[3,4] This procedure has enabled the realization of different types of carbon nanomaterials such as nanographenes,[5] graphene nanoribbons (GNRs),[6] nanoporous graphenes (NPGs),[7,8] 1D conjugated polymers (1DCPs)[9,10] and 2D conjugated polymers (2DCPs).[11,12] *Via* the rational design of organic building blocks it has been possible to fine-tune the electronic and magnetic properties of the resulting nanomaterials. Examples of this approach are GNRs and 1DCPs, where topological phases (*e.g.* trivial and non-trivial states) have been realized by carefully designing their atomic structure.[9,13–15] Both topological GNRs and 1DCPs are promising candidates for future

carbon-based quantum electronics, which is a branch of advanced electronics that aims at exploiting quantum phenomena in molecular scale organic systems for novel device applications.[16,17]

In this regard, an interesting class of 1DCPs are those based on triarylmethyls (TAMs). TAMs are a well-known family of π-conjugated organic radicals composed of three aryl rings bound to a central carbon atom (αC), where their unpaired electron mainly resides.[18,19] Due to their fully π-conjugated structure, the unpaired electron (and associated spin) is partially delocalized throughout the molecule. The degree of spin delocalization mainly depends on the dihedral angle of the three aryl rings in every TAM.[20] TAMs have been used as building blocks of diverse multifunctional materials,[19] such as magnetic metal–organic frameworks,[21] magnetic 1DCPs,[18,22] electro-switchable self-assembled monolayers[23] and, more recently, antiferromagnetic (AFM) 2DCPs.[24,25] TAM 1DCPs, concretely, may be classified depending on how adjacent αCs are connected along the 1D chain. If αCs are connected in a meta-configuration, the associated spins tend to be ferromagnetically (FM) coupled.[26] Because of this, such *meta*-1DCPs were intensively studied as organic magnets a few decades ago.[18,22] At the same time, the *meta*-configuration also electronically isolates all unpaired electrons, making the resulting 1DCPs electrical insulators. In contrast, connecting αCs in a *para*-configuration enables both a magnetic and electronic coupling of the π-conjugated unpaired electrons.[27–29] Such a

[a] *Departament de Ciència de Materials i Química Física & Institut de Química Teòrica i Computacional (IQTCUB), Universitat de Barcelona, c/Martí i Franquès 1-11, 08028 Barcelona, Spain. E-mail: ialcon@ub.edu*

[b] *Institució Catalana de Recerca i Estudis Avançats (ICREA), Passeig Lluís Companys 23, 08010 Barcelona, Spain*

8618 | *Phys. Chem. Chem. Phys.*, 2026, **28**, 8618–8625

This journal is © the Owner Societies 2026

configuration leads to an interplay between a multiradical AFM solution and a closed-shell quinoidal (QUI) solution,[29] in line with the behaviour of the corresponding TAM dimers (*e.g.* Thiele's and Tschitschibabin's hydrocarbons)[30] and 2DCPs.[31,32] As demonstrated in earlier work on molecular conjugated hydrocarbons, the interplay between the AFM and QUI solutions is primarily governed by the competition between aromaticity and bond pairing.[33] Interestingly, it has recently been predicted that the electron-paired QUI phase in these *para*-connected 1DCPs may lead to topologically protected non-trivial end states in the corresponding oligomers,[34] increasing the potential of TAM 1DCPs for quantum electronics.[16] However, to date, control over the ground-state of such 1DCPs is still limited, and reliable design strategies to impose a specific quantum state (*i.e.* AFM or QUI) are necessary for the future application of these correlated 1D systems in advanced quantum technologies.

Here, *via* first principles density functional theory (DFT) simulations, we have studied the electronic and magnetic properties of *para*-connected TAM-based mixed-valence 1DCPs (mv-1DCPs) obtained *via* a rational substitution of selected αC centres along the 1DCP chain by nitrogen (N) atoms. Such N substitutions may be regarded as an effective local addition of an extra π-conjugated electron, thus quenching any spin density at the substituted site. We evaluate two simple periodic N-patterns which, in principle, could be realized *via* bottom-up assembly of TAM and triarylamine (TAA) units. Specifically, we consider: (i) a fully-alternating mv-1DCP, referred to as NCNC-1DCP, and (ii) a 2-by-2 alternating mv-1DCP, which we label as NNCC-1DCP. Our findings show that in NCNC-1DCP the two αC

unpaired electrons cannot pair, due to the presence of the substitutional N atoms in between them; leading to a pure multiradical open-shell state. We observe that the two αC spin centres are AFM coupled, with an energetically less stable FM configuration which displays an increased band dispersion. Conversely, in the NNCC-1DCP, the αCs are directly connected *via* a single phenyl-ring and our simulations reveal that this N-substitution pattern leads to an effective electron pairing, as evidenced by the complete disappearance of any spin signal. Finally, *ab initio* molecular dynamics (AIMD) simulations show that these electronic configurations are robust under thermally induced structural fluctuations at 300 K. In turn these AIMD calculations provide insight into how each electronic phase (*e.g.* AFM or QUI) influences the dynamic structural behaviour of the corresponding mv-1DCP system.

Results and discussion

The mv-1DCPs to be studied in this work are based on the ring-sharing TAM 1DCP shown in Fig. 1a, where vertical dashed lines indicate the boundaries of the periodic unit cell of the system. Having only one phenyl ring between the αC centres enhances their electronic coupling, which is important for applications in electronics.[35] Additionally, ring-sharing TAM dimers and nanorings have already been experimentally reported,[18,36] which supports the experimental feasibility of this type of systems. In the TAM 1DCP shown in Fig. 1a, which is based on triphenylmethyl (TPM), two competing electronic
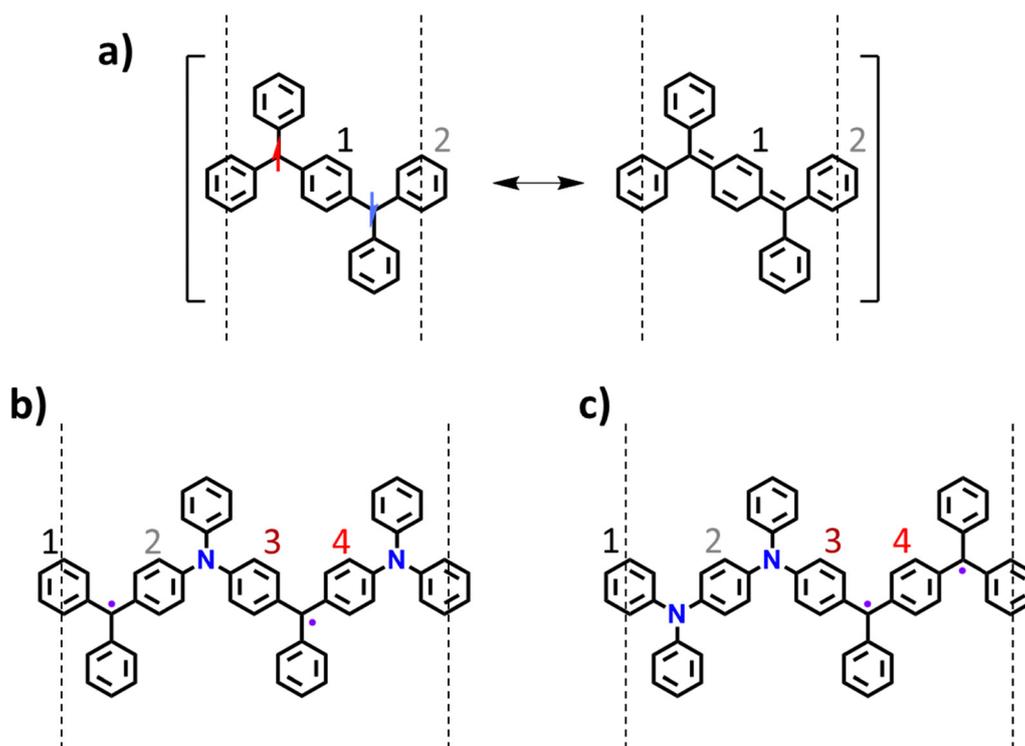

Fig. 1 (a) Chemical sketch of the TPM 1DCP where an interplay between a multiradical AFM and closed–shell QUI configurations takes place at room temperature.[29] Chemical sketches of the two proposed mv-1DCPs, namely (b) the NCNC-1DCP and (c) the NNCC-1DCP.

This journal is © the Owner Societies 2026

Phys. Chem. Chem. Phys., 2026, **28**, 8618–8625 | **8619**

configurations are observed—namely, the multiradical AFM and the closed-shell QUI states—as is also the case with the corresponding 2D analogues.[31,32] As predicted for the molecular derivatives, a single phenyl ring between the two αC centres promotes the QUI state.[33] Having more phenyl rings between αC centres promotes a biradical character due to the associated increased stabilization *via* aromatization.[33] In TAM 1DCPs, such two electronic solutions (see Fig. 1a) have been predicted to be dynamically inter-changing at 300 K, driven by thermal fluctuations.[29] Here, we explore the possibility to tune the relative stability of these different states by means of periodic substitutions of αC nodes by N nodes. Substitution of αC nodes by N nodes was similarly exploited to tune the electronic structure of TAM 2DCPs, and was shown to induce a robust multiradical ground-state and magnetic frustration.[37] Inspired by this, here we focus on two mv-1DCPs with two distinct alternating N-substitution patterns (*i.e.* NCNC-1DCP and NNCC-1DCP, as shown in Fig. 1b and 1c, respectively). These mv-1DCPs are simulated with DFT calculations employing the hybrid PBE0 functional[38] as implemented in the all-electron FHI-AIMS code[39] (see Methods for further details).

The NCNC-1DCP optimized structure in its ground-state is shown in Fig. 2a, where it may be seen that all aryl rings along the chain (*i.e.* those responsible for electron dispersion) are equally twisted (see side view in Fig. 2a) with an average dihedral of about 37.5° (more details below). This dihedral angle is significantly larger than that reported for the parent TPM 1DCP ($\sim 26°$)[29] which may originate from a higher electron localization in the NCNC-1DCP (see below). By inspecting the corresponding spatially-resolved spin-density map we see that the ground-state displays an AFM alignment with respect to the αC nodes. As expected, no spin density originates from the N sp^2

centres (purple sites in Fig. 2b), consistent with their closed-shell character. The band structure of this multiradical AFM state displays nearly flat valence and conduction bands being separated by a band gap of 2 eV (Fig. 2c), which is in striking contrast to the TPM 1DCP (Fig. 1a) which was shown to display much higher dispersion (*ca.* 1 eV).[29] This indicates that N-substitutions in the NCNC-1DCP block the delocalization of αC unpaired electrons along the chain, giving rise to their nearly flat bands. This result is also in full agreement with high dihedral angles in the NCNC-1DCP as compared to TPM 1DCP (see above) which cannot be attributed to steric hindrance effects since the two systems are equally based on phenyl rings.

A ferromagnetic (FM) alignment of αCs spins may also be stabilized in the NCNC-1DCP, as shown in Fig. 2d. The FM and AFM configurations display nearly identical geometries (see Fig. S1 in the SI) and we find that the FM configuration is sitting 24.5 meV above the AFM state (note that ΔE_{FM-AFM} is normalized per αC centre). This ΔE_{FM-AFM} translates into a magnetic coupling constant (J) of -49 meV (see Methods for details) which is very much in line with that of N-substituted mv-2DCPs (-46 meV).[37] As it may be seen in Fig. 2e, the FM alignment of unpaired electrons on the αC centres splits the bands according to their spin, leading to a valence (conduction) band being purely spin-up (spin-down) polarized. Additionally, both sets of bands display a significant increase in band dispersion as compared to the AFM ground-state (Fig. 2c), and their energy difference (*i.e.* the band gap) is also reduced to 1.7 eV (Fig. 2e). While the combination of these factors could be promising for spintronics (purely spin-polarized bands with significant band dispersion), at room temperature, where $k_B T = 25$ meV, only a fraction of the system would be populated to the FM phase, and so a minor improvement in quantum
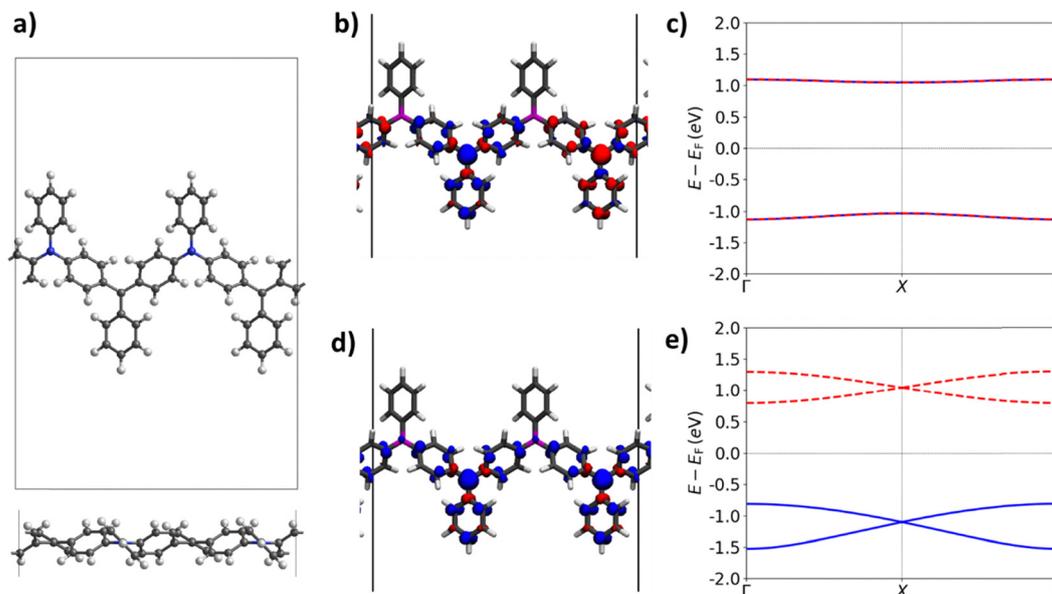

Fig. 2 (a) Top and side views of the optimized atomic structure of NCNC–1DCP in the AFM configuration. Spatially-resolved spin density in (b) the AFM and (d) FM configurations (iso-value: 0.005 e Bohr^{-3}), displaying their associated band structures in (c) and (e), respectively. Spin-up and spin down electron densities (bands) are depicted in blue and red, respectively.

8620 | *Phys. Chem. Chem. Phys.*, 2026, **28**, 8618–8625

This journal is © the Owner Societies 2026

transport should be expected (*i.e.* with respect to the electrically insulating AFM ground-state; Fig. 2c).

Moving to the NNCC-1DCP, we show the corresponding fully optimized structure in Fig. 3a. Here we see a key distinction with the NCNC-1DCP: namely, that all in-chain aryl rings are equally twisted except one, which appears to be significantly flatter than the rest (see red arrow in Fig. 3a). This different behaviour between the NCNC-1DCP and the NNCC-1DCP is clearly visible by plotting the dihedral angles for all four in-chain aryl rings for each system. As shown in Fig. S2, NCNC-1DCP displays a homogeneous distribution of dihedral angles around 37°, regardless of the magnetic configuration (AFM or FM). However, the NNCC-1DCP displays dihedral angles well-above 40°, and one aryl ring being rotated by only 16°. The flattened phenyl ring sits between the two αC centres (Fig. 3a), which points to a likely effective electron-pairing (of the otherwise αCs' unpaired electrons) within that ring. Indeed, a null spin polarization is obtained for the NNCC-1DCP (Fig. S3), demonstrating the closed-shell nature of this system. By plotting the density of the highest occupied crystal orbital (HOCO), shown in Fig. 3b, we observe the formation of a QUI-type electron paired configuration along the flattened phenyl ring. This is further supported by analysing the bond-length alternation (BLA) for each phenyl ring along the chain, as shown in Fig. S4. Here we see that while most aryl rings display rather low BLA values of *ca.* 0.025 Å, compatible with a

moderate degree of aromatization, the flattened aryl ring possesses a BLA value of 0.097 Å. Such a high BLA is very close to that of para-quinodimethane (BLA = 0.11 Å)[33] and confirms the complete quinonization of that ring. Since all rings are phenyl rings (*i.e.* with hydrogen-functionalized edges) they necessarily experience the same degree of steric hindrance, as clearly evidenced in the side view of the NCNC-1DCP geometry shown in Fig. 2a. Because of this, we conclude that the flattening of ring #4 in the NNCC-1DCP originates from the electronic pairing mechanism (*i.e.* quinonization) and the associated formation of C–C double bonds between ring #4 and the adjacent αC atoms (see Fig. S5). These double bonds become more stabilized as the phenyl ring becomes more coplanar with respect to the sp² plane of the αCs, due to a higher π–π orbital overlap.

The corresponding band structure, shown in Fig. 3c, displays a rather flat conduction band and a slightly more dispersive valence band. Overall, the flatness of the bands for the NNCC-1DCP fully agrees with the conclusion extracted from NCNC-1DCP results (Fig. 2c) – namely, that N-substitutions tend to localize αC unpaired electrons as compared to the non-substituted case (*i.e.* the TPM 1DCP[29]). Previous theoretical studies on the molecular analogues showed that a higher electron localization promotes the electron-paired QUI configuration,[33] which is in good agreement with the QUI ground-state we find in the NNCC-1DCP (Fig. 3).

Up to now we have shown that one may use a rational N-substitution of αC centres to tune the mv-1DCP ground state,
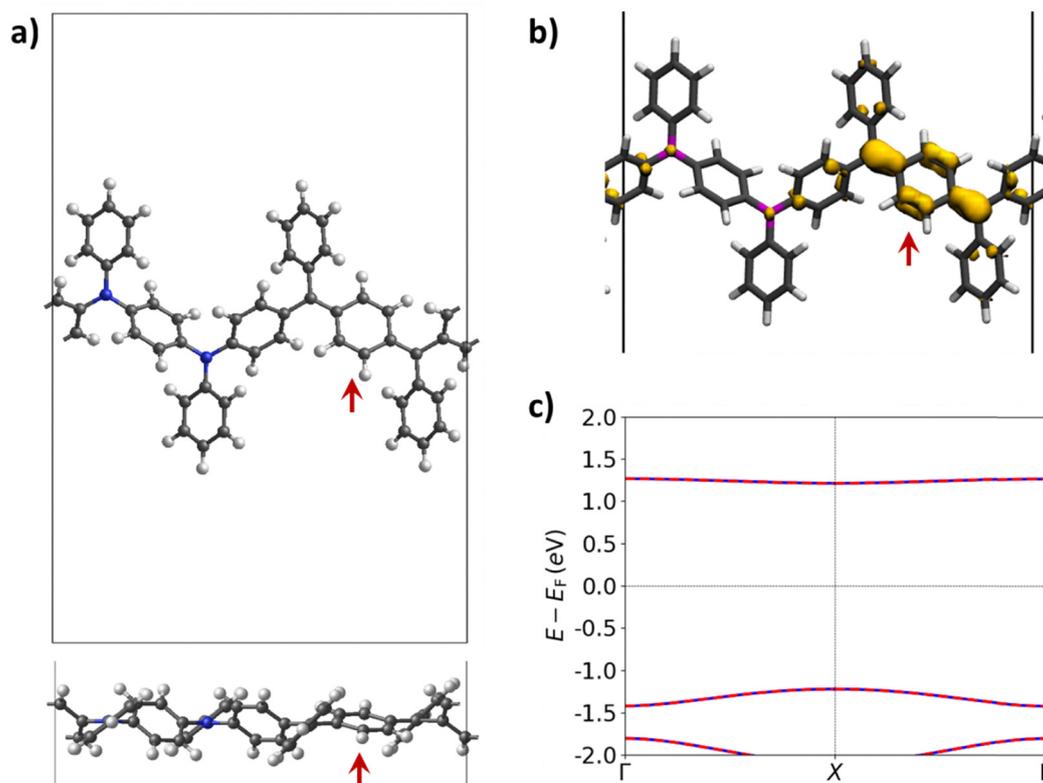

Fig. 3 (a) Top and side views of the optimized atomic structure of the NNCC-1DCP, (b) spatially-resolved eigenstate density of the HOCO (iso-value: 0.002 e Bohr^{-3}), and (c) corresponding band structure. Red arrows in (a) and (b) indicate the position of the flatter phenyl ring in the polymer. Spin-up and spin down bands are depicted in blue and red, respectively.

This journal is © the Owner Societies 2026

Phys. Chem. Chem. Phys., 2026, **28**, 8618–8625 | **8621**

via a localization of the remaining αC π-conjugated electrons, as evidenced by the corresponding band structures. Semi-alternant distributions (*i.e.* NNCC-1DCP) enable the formation of a closed-shell Kekulé configuration, as represented in Fig. S5, which appears to be the ground-state solution (Fig. 3). On the contrary, a fully alternated distribution of N sites (*i.e.* NCNC-1DCP) does not allow such an electron-paired configuration, and instead results in a purely open-shell multi-radical ground-state (Fig. 2). These characteristics, however, could be susceptible to dynamic changes under thermal fluctuations at finite temperature, as previously found for TAM 2DCPs.[32] To assess the robustness of our results under more realistic conditions, we have conducted AIMD simulations to evaluate the behaviour of mv-1DCPs at 300 K (see Methods for details). As a reference point, we use the non-substituted TPM 1DCP (Fig. 1a) whose behaviour at 300 K was theoretically studied by some of us in a prior study.[29] In the following, we thus compare the two mv-1DCPs with the TPM 1DCP (Fig. 4).

To follow the time-evolution of the electronic structure we use the mean of the absolute spin population on the αC centres, which are the atoms mainly hosting the unpaired electrons in the multiradical state (see Fig. 2b and d). Since our considered mv-1DCPs contain two αC centres per unit cell (as the TPM 1DCP), this quantity is calculated as $\langle|\mu_{\alpha C}|\rangle = (|\mu_{\alpha C1}| + |\mu_{\alpha C2}|)/2$, where $|\mu_{\alpha C1}|$ and $|\mu_{\alpha C2}|$ are the absolute values of spin populations in αC_1 and αC_2, respectively. Additionally, due to the direct correlation between in-chain aryl rings twisting and electron-pairing, we also analyse the evolution of in-chain dihedral angles throughout the AIMD run for each system (see bottom panels in Fig. 4). The TPM 1DCP displays a dynamic electron-pairing/unpairing process, which leads to a constant and uninterrupted fluctuation of $\langle|\mu_{\alpha C}|\rangle$

between 0.25 and zero (Fig. 4b). Fast fluctuations of $\langle|\mu_{\alpha C}|\rangle$, with an oscillation period of a few tens of femtoseconds, were previously shown to originate from bond vibrations.[29] However, if in-chain aryl rings 1 and 2 are partially twisted (see Fig. 1a for labelling), as it occurs at the crossing point of their corresponding dihedral angles (see region between vertical dashed red lines in Fig. 4e), a "sustained" $\langle|\mu_{\alpha C}|\rangle$ signal emerges associated with a brief stabilization of the multiradical AFM state (see region between vertical dashed red lines in Fig. 4b).

Conversely, as shown in Fig. 4a, the NCNC-1DCP displays a stable and significantly higher $\langle|\mu_{\alpha C}|\rangle$ signal throughout the entire AIMD run, corresponding to a very robust multiradical solution at 300 K. This is consistent with the purely open-shell character of NCNC-1DCP obtained at 0 K (Fig. 2). Therefore, the alternant distribution of N atoms shown in Fig. 1b effectively prevents the unpaired electrons along the 1D chain to hybridize, forcing them to remain unpaired even under strong structural fluctuations at 300 K. The lack of any local electron pairing process gives rise to similar rotation profiles for all in-chain aryl rings (see labels 1–4 in Fig. 1b) without notable changes in their rotational behaviour during the AIMD run (see Fig. 4d). Their mean dihedral angle sits between 38 and 39° for all rings (see Table S1), as typically obtained for those phenyl rings not hosting any QUI electron pairing (see for *e.g.* TPM 1DCP's φ_1 - black curve - for the first two picoseconds in Fig. 4e).

Moving to the NNCC-1DCP, we may observe a very different picture. First of all, this mv-1DCP displays a zero value in $\langle|\mu_{\alpha C}|\rangle$ for most of the AIMD run (see Fig. 4c) with sudden peaks which we associate to rapid electron unpairing/pairing processes induced by bond vibrations, as previously demonstrated for the TPM 1DCP.[29] Therefore, the NNCC-1DCP displays a rather robust closed-shell QUI electron-paired configuration, due to
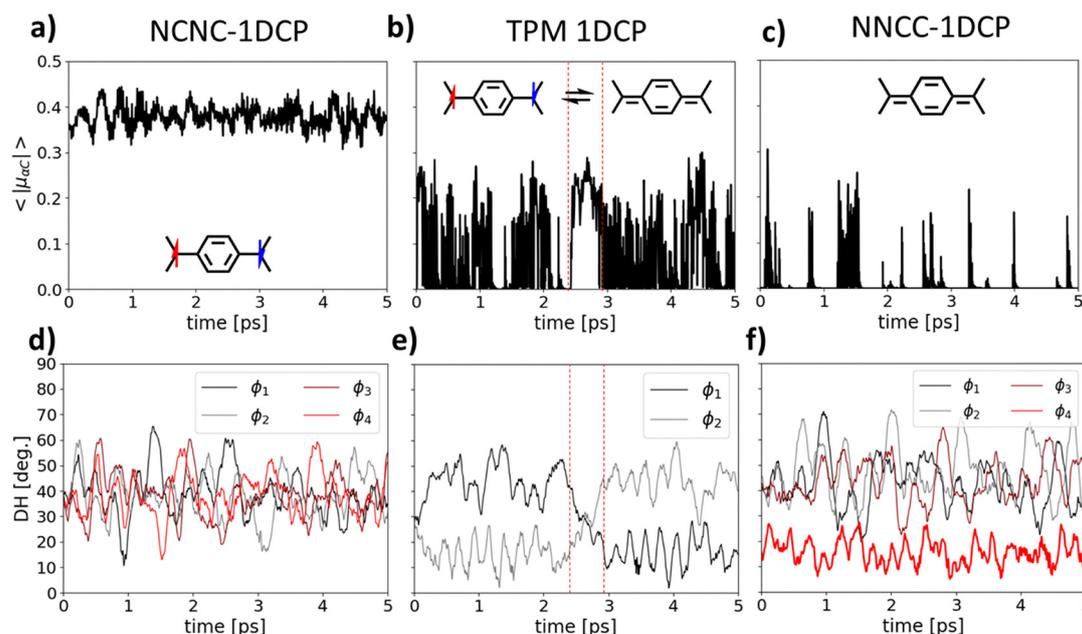

Fig. 4 Time-resolved evolution of $|\mu_{aC}|$ for a) the NCNC-1DCP, b) the TPM 1DCP and c) the NNCC-1DCP during a 5 ps AIMD run at 300 K (see Methods for details), and d)–f) corresponding time-resolved dihedral angle for every in-chain phenyl ring, φ_i (see Fig. 1 for phenyl ring indices).

8622 | *Phys. Chem. Chem. Phys.*, 2026, **28**, 8618–8625

This journal is © the Owner Societies 2026

the direct coupling of the two αC centres *via* a single phenyl ring, which is further supported by the sustained high BLA value for ring #4 shown in Fig. S6b, in turn being in full agreement with our findings at 0 K (Fig. S4). This phenyl ring (#4 in Fig. 1c) also displays a steadily flatter conformation ($\langle \varphi \rangle \approx 15°$) during the entire AIMD run (see red curve in Fig. 4f) as compared to the other in-chain phenyl rings with average dihedrals between 43 and 48° (see Table S1). The flatter phenyl ring also displays a significantly lower rotation throughout the run, as reflected in a dihedral angle standard deviation (σ_φ) being nearly half that of the other rings (Table S1). These low $\langle \varphi \rangle$ and σ_φ values originate from the electron-paired QUI configuration which becomes more stabilized the more coplanar the local π-conjugated system is. We also note that similar $\langle \varphi \rangle$ and σ_φ values are observed for those phenyl rings temporarily hosting the electron pairing in the TPM 1DCP (see the grey curve for the first two picoseconds, or the black curve for the last two picoseconds in Fig. 4e). Therefore, we may see how the quantum ground-state of TAM 1DCPs, as engineered *via* a rational N-substitution, determines not only their structural conformation (*i.e.* $\langle \varphi \rangle$) but also their dynamic behaviour at finite temperature – *e.g.* a more, or less, facile rotation of phenyl rings (Fig. 4d–f).

Conclusions

In this work we have shown that the quantum electronic state of 1DCPs may be tuned *via* a rational substitution of sp^2 αC nodes by N atoms. Concretely, we have considered N-substitutions arranged in two simple distributions which lead to unpaired (NCNC-1DCP) or paired (NNCC-1DCP) π-conjugated electrons.

The fully alternating NCNC-1DCP stabilizes a multiradical open-shell electronic configuration with an AFM ground-state and a FM solution sitting 24.5 meV (per αC node) above it. This FM configuration displays a purely spin-polarized valence (spin up) and conduction (spin down) band and a significantly higher band dispersion as compared to the insulating AFM ground-state. The energy difference between the AFM and FM configurations indicates a non-negligible population of the FM phase at room temperature, which could induce a slight improvement in the conductivity of the NCNC-1DCP under such conditions.

On the other hand, a semi-alternating distribution of N atoms, as in the NNCC-1DCP, stabilizes a robust electron-paired configuration. This arises from the direct coupling of the two αC sites *via* a single phenyl ring, which enables the pairing of their otherwise unpaired electrons, as corroborated by the spatial distribution of the HOCO density. Such electron pairing leads to the flattening of the phenyl ring hosting it, and to the lack of any spin density, demonstrating the closed-shell nature of the system. The corresponding band structure displays a flat conduction band and a weakly dispersive valence band, which agrees with the rather localized nature of this electron-paired QUI state.

Finally, we have also evaluated the robustness of this chemically-inspired quantum engineering strategy to thermal fluctuations at 300 K *via* AIMD simulations. In the NCNC-1DCP a high value of $\langle |\mu_{\alpha C}| \rangle$ is stabilized throughout the AIMD run, which demonstrates that the electron-pairing mechanism is completely deactivated by the presence of N atoms in such fully alternating fashion. On the contrary, the NNCC-1DCP displays a nearly complete depletion of the $\langle |\mu_{\alpha C}| \rangle$ signal, which is attributed to a robust electron-paired configuration. Random $\langle |\mu_{\alpha C}| \rangle$ peaks though appear throughout the run, which arise from rapid C–C bond vibrations as previously demonstrated for the parent TPM 1DCP.[29] This robust electron-paired configuration is reflected in the conformation of the polymer: the phenyl ring hosting the electron pairing gets significantly flatter than the other phenyl rings and also more rigid (*i.e.* less prone to rotation). None of this is observed for the purely open-shell NCNC-1DCP. Our findings thus demonstrate that N-substitution allows for tuning of the quantum ground-state of 1DCPs which, in turn, influences their molecular conformation even under thermal fluctuations at room temperature. Therefore, we believe that the ideas herein proposed could inspire the future design of carbon-based nanomaterials for quantum electronics and spintronics.

Methods

The atomic structures of mv-1DCPs have been constructed from a previously optimized TPM 1DCP periodic model[29] by repeating the unit cell one time along the polymer direction (x direction) and making N-substitutions in the appropriate locations to obtain the NCNC-1DCP and NNCC-1DCP, respectively. The atomic structure of each polymer has been optimized using DFT calculations employing the PBE0 hybrid functional[38] and using a Tier-1 light numerical atom-centered orbital (NAO) basis set,[40] as implemented in the Fritz Haber Institute *ab initio* molecular simulations package (FHI-AIMS).[39,41] We note that the PBE0 functional has been shown to provide reliable results for other TAM-based materials, such as TAM molecular nanorings and 2DCPs.[32,37,42,43] All calculations have been performed using spin-unrestricted DFT calculations and setting an anti-parallel spin initial guess between neighbouring αC nodes, in order to ensure that multiradical solutions were found whenever possibly stabilized in each system. All calculations employed a $3 \times 1 \times 1$ Γ-centred Monkhorst–Pack (MP) k-mesh, and a convergence criterion of 1×10^{-5} eV for the total energy and 1×10^{-2} eV Å^{-1} for the maximum force component per atom. During these optimizations, the a unit cell parameter (x-direction) was also minimized, while fixing the vacuum level along y- and z-directions. Subsequently, single-point calculations were performed using the fully optimized structures to calculate the electronic structure of each system using the above settings but with a $9 \times 1 \times 1$ MP k-mesh. From these single-point calculations we have extracted total energies, spatially resolved electron density maps and electronic band structures. The Hirshfeld method was used to extract atomically-partitioned spin populations (μ_i).[44] Magnetic coupling constants have been calculated as follows:

$$J = E_{\text{AFM}} - E_{\text{FM}}, \tag{1}$$

This journal is © the Owner Societies 2026

Phys. Chem. Chem. Phys., 2026, **28**, 8618–8625 | **8623**

By assuming the following spin Hamiltonian:

$$\hat{H} = \sum_{i>j} -J\hat{S}_{z,i}\hat{S}_{z,j}, \tag{2}$$

where $\hat{S}_z$ is the operator for the spin z-component and the summation runs only for the (spin-polarized) αC centres within the unit cell.

Finally, we have computed 5 picosecond AIMD runs to simulate the atomic and electronic structure of mv-1DCPs at 300 K using the FHI-AIMS code. Here, we used the Bussi–Donadio–Parrinello thermostat[45] and the same DFT settings as for the 0 K optimisations.

Conflicts of interest

There are no conflicts of interest to declare.

Data availability

Data for this article, including optimization and single-point input and output files, is available in Zenodo at https://doi.org/10.5281/zenodo.17752453.

Supplementary information (SI) is available. See DOI: https://doi.org/10.1039/d5cp04664e.

Acknowledgements

References

1 L. Grill, M. Dyer, L. Lafferentz, M. Persson, M. V. Peters and S. Hecht, Nano-architectures by covalent assembly of molecular building blocks, *Nat. Nanotechnol.*, 2007, **2**, 687–691.

2 J. Cai, P. Ruffieux, R. Jaafar, M. Bieri, T. Braun, S. Blankenburg, M. Muoth, A. P. Seitsonen, M. Saleh, X. Feng, K. Müllen and R. Fasel, Atomically precise bottom-up fabrication of graphene nanoribbons, *Nature*, 2010, **466**, 470–473.

3 X. H. Liu, C. Z. Guan, D. Wang and L. J. Wan, Graphene-like single-layered covalent organic frameworks: synthesis strategies and application prospects, *Adv. Mater.*, 2014, **26**, 6912–6920.

4 G. Y. Xing, Y. C. Zhu, D. Y. Li and P. N. Liu, On-Surface Cross-Coupling Reactions, *J. Phys. Chem. Lett.*, 2023, **14**, 4462–4470.

5 A. Narita, X.-Y. Wang, X. Feng and K. Müllen, New advances in nanographene chemistry, *Chem. Soc. Rev.*, 2015, **44**, 6616–6643.

6 X. Zhou and G. Yu, Modified Engineering of Graphene Nanoribbons Prepared via On-Surface Synthesis, *Adv. Mater.*, 2020, **32**, 1905957.

7 T. Qin, T. Wang and J. Zhu, Recent progress in on-surface synthesis of nanoporous graphene materials, *Commun. Chem.*, 2024, **7**, 154.

8 I. Alcón, A. W. Cummings, E. Ribas, S. Roche and A. Mugarza, Progress on quantum transport engineering in atomically precise anisotropic nanoporous graphene, *Nanoscale Adv.*, 2025, **7**, 5932–5943.

9 B. Cirera, A. Sánchez-Grande, B. de la Torre, J. Santos, S. Edaltamanesh, E. Rodríguez-Sánchez, K. Lauwaet, B. Mallada, R. Zbořil, R. Miranda, O. Gröning, P. Jelínek, N. Martín and D. Ecija, Tailoring topological order and π-conjugation to engineer quasi-metallic polymers, *Nat. Nanotechnol.*, 2020, **15**, 437–443.

10 K. Sun, N. Cao, O. J. Silveira, A. O. Fumega, F. Hanindita, S. Ito, J. L. Lado, P. Liljeroth, A. S. Foster and S. Kawai, On-surface synthesis of Heisenberg spin-1/2 antiferromagnetic molecular chains, *Sci. Adv.*, 2025, **11**, eads1641.

11 G. Galeotti, F. De Marchi, E. Hamzehpoor, O. MacLean, M. Rajeswara Rao, Y. Chen, L. V. Besteiro, D. Dettmann, L. Ferrari, F. Frezza, P. M. Sheverdyaeva, R. Liu, A. K. Kundu, P. Moras, M. Ebrahimi, M. C. Gallagher, F. Rosei, D. F. Perepichka and G. Contini, Synthesis of mesoscale ordered two-dimensional π-conjugated polymers with semiconducting properties, *Nat. Mater.*, 2020, **19**, 874–880.

12 Q. Fan, L. Yan, M. W. Tripp, O. Krejčí, S. Dimosthenous, S. R. Kachel, M. Chen, A. S. Foster, U. Koert, P. Liljeroth and J. M. Gottfried, Biphenylene network: A nonbenzenoid carbon allotrope, *Science*, 2021, **372**, 852–856.

13 O. Gröning, S. Wang, X. Yao, C. A. Pignedoli, G. Borin Barin, C. Daniels, A. Cupo, V. Meunier, X. Feng, A. Narita, K. Müllen, P. Ruffieux and R. Fasel, Engineering of robust topological quantum phases in graphene nanoribbons, *Nature*, 2018, **560**, 209–213.

14 D. J. Rizzo, G. Veber, T. Cao, C. Bronner, T. Chen, F. Zhao, H. Rodriguez, S. G. Louie, M. F. Crommie and F. R. Fischer, Topological band engineering of graphene nanoribbons, *Nature*, 2018, **560**, 204–208.

15 H. González-Herrero, J. I. Mendieta-Moreno, S. Edaltamanesh, J. Santos, N. Martín, D. Écija, B. Torre and P. Jelinek, Atomic Scale Control and Visualization of Topological Quantum Phase Transition in π-Conjugated Polymers Driven by Their Length, *Adv. Mater.*, 2021, **33**, 2104495.

16 H. Wang, H. S. Wang, C. Ma, L. Chen, C. Jiang, C. Chen, X. Xie, A. P. Li and X. Wang, Graphene nanoribbons for quantum electronics, *Nat. Rev. Phys.*, 2021, **3**, 791–802.

17 F. Lombardi, A. Lodi, J. Ma, J. Liu, M. Slota, A. Narita, W. K. Myers, K. Müllen, X. Feng and L. Bogani, Quantum units from the topological engineering of molecular graphenoids, *Science*, 2019, **366**, 1107–1110.

18 N. M. Shishlov, From the Gomberg radical to organic magnets, *Russ. Chem. Rev.*, 2006, **75**, 863–884.

19 I. Ratera, J. Vidal-Gancedo, D. Maspoch, S. T. Bromley, N. Crivillers and M. Mas-Torrent, Perspectives for polychlorinated trityl radicals, *J. Mater. Chem. C*, 2021, **9**, 10610–10623.

8624 | *Phys. Chem. Chem. Phys.*, 2026, **28**, 8618–8625

This journal is © the Owner Societies 2026

20 I. Alcón and S. T. Bromley, Structural Control over Spin Localization in Triarylmethyls, *RSC Adv.*, 2015, **5**, 98593–98599.

21 D. Maspoch, D. Ruiz-Molina, K. Wurst, N. Domingo, M. Cavallini, F. Biscarini, J. Tejada, C. Rovira and J. Veciana, A nanoporous molecular magnet with reversible solvent-induced mechanical and magnetic properties, *Nat. Mater.*, 2003, **2**, 190–195.

22 A. Rajca, J. Wongsriratanakul and S. Rajca, Magnetic ordering in an organic polymer, *Science*, 2001, **294**, 1503–1505.

23 C. Simão, M. Mas-Torrent, N. Crivillers, V. Lloveras, J. M. Artés, P. Gorostiza, J. Veciana and C. Rovira, A robust molecular platform for non-volatile memory devices with optical and magnetic responses, *Nat. Chem.*, 2011, **3**, 359–364.

24 J. Wu, S. Wu, M. Li, H. Phan, D. Wang, T. S. Herng, J. Ding and Z. Lu, Toward π-Conjugated 2D Covalent Organic Radical Frameworks, *Angew. Chem., Int. Ed.*, 2018, **57**, 8007–8011.

25 Y. Yang, C. Liu, X. Xu, Z. Meng, W. Tong, Z. Ma, C. Zhou, Y. Sun and Z. Sheng, Antiferromagnetism in two-dimensional polyradical nanosheets, *Polym. Chem.*, 2018, **9**, 5499–5503.

26 D. R. Mañeru, I. de, P. R. Moreira and F. Illas, Helical Folding-Induced Stabilization of Ferromagnetic Polyradicals Based on Triarylmethyl Radical Derivatives, *J. Am. Chem. Soc.*, 2016, **138**, 5271–5275.

27 D. Braun and P. Lehmann, Stabile Polykohlenstoffradikale, 2. Versuche zur Darstellung von Polyradikalen des Triphenylmethyl-Typs, verknüpft über p-Phenylen-Einheiten, *Makromol. Chem.*, 1976, **177**, 1387–1400.

28 K. Yoshizawa and R. Hoffmann, Potential Linear-Chain Organic Ferromagnets, *Chem. – Eur. J.*, 1995, **1**, 403–413.

29 I. Alcón, J. Shao, J. C. Tremblay and B. Paulus, Conformational control over π-conjugated electron pairing in 1D organic polymers, *RSC Adv.*, 2021, **11**, 20498–20506.

30 L. K. Montgomery, J. C. Huffman, E. A. Jurczak and M. P. Grendze, The molecular structures of Thiele's and Chichibabin's hydrocarbons, *J. Am. Chem. Soc.*, 1986, **108**, 6004–6011.

31 I. Alcón, F. Viñes, I. de, P. R. Moreira and S. T. Bromley, Existence of multi-radical and closed-shell semiconducting states in post-graphene organic Dirac materials, *Nat. Commun.*, 2017, **8**, 1957.

32 I. Alcón, R. Santiago, J. Ribas-Arino, M. Deumal, I. de, P. R. Moreira and S. T. Bromley, Controlling pairing of π-conjugated electrons in 2D covalent organic radical frameworks *via* in-plane strain, *Nat. Commun.*, 2021, **12**, 1705.

33 G. Trinquier and J.-P. Malrieu, Kekulé versus Lewis: when aromaticity prevents electron pairing and imposes polyradical character, *Chem. – Eur. J.*, 2015, **21**, 814–828.

34 I. Alcón, L. M. Canonico, N. Papior, J. Garcia, A. W. Cummings, J. Tremblay, M. Pruneda, M. Brandbyge, B. Paulus and S. Roche, Twisting Between Topological Phases in 1D Conjugated Polymers *via* a Multiradical Transition State, *Adv. Funct. Mater.*, 2024, **34**, 2409174.

35 J. Shao, I. Alcón, B. Paulus and J. C. Tremblay, Understanding Charge Transport in Triarylmethyl-Based Spintronic Nanodevices, *J. Phys. Chem. C*, 2021, **125**, 25624–25633.

36 Z. Li, T. Y. Gopalakrishna, Y. Han, Y. Gu, L. Yuan, W. Zeng, D. Casanova and J. Wu, Cyclo-para-phenylmethine: An Analog of Benzene Showing Global Aromaticity and Open-shell Diradical Character, *J. Am. Chem. Soc.*, 2019, **141**, 16266–16270.

37 I. Alcón, J. Ribas-Ariño, I. de, P. R. Moreira and S. T. Bromley, Emergent Spin Frustration in Neutral Mixed-Valence 2D Conjugated Polymers: A Potential Quantum Materials Platform, *J. Am. Chem. Soc.*, 2023, **145**, 5674–5683.

38 C. Adamo and V. Barone, Toward reliable density functional methods without adjustable parameters: The PBE0 model, *J. Chem. Phys.*, 1999, **110**, 6158.

39 V. Blum, R. Gehrke, F. Hanke, P. Havu, V. Havu, X. Ren, K. Reuter and M. Scheffler, Ab initio molecular simulations with numeric atom-centered orbitals, *Comput. Phys. Commun.*, 2009, **180**, 2175–2196.

40 I. Y. Zhang, X. Ren, P. Rinke, V. Blum and M. Scheffler, Numeric atom-centered-orbital basis sets with valence-correlation consistency from H to Ar, *New J. Phys.*, 2013, **15**, 123033.

41 V. Havu, V. Blum, P. Havu and M. Scheffler, Efficient O(N) integration for all-electron electronic structure calculation using numeric basis functions, *J. Comput. Phys.*, 2009, **228**, 8367–8379.

42 I. Alcón, D. Reta, I. de, P. R. Moreira and S. T. Bromley, Design of multi-functional 2D open-shell organic networks with mechanically controllable properties, *Chem. Sci.*, 2017, **8**, 1027–1039.

43 R. Santiago, I. Alcón, J. Ribas-Arino, M. Deumal, I. P. R. Moreira and S. T. Bromley, 2D Hexagonal Covalent Organic Radical Frameworks as Tunable Correlated Electron Systems, *Adv. Funct. Mater.*, 2020, **31**, 2004584.

44 F. L. Hirshfeld, Bonded-atom fragments for describing molecular charge densities, *Theor. Chem. Acc.*, 1977, **44**, 129–138.

45 G. Bussi, D. Donadio and M. Parrinello, Canonical sampling through velocity rescaling, *J. Chem. Phys.*, 2007, **126**, 014101.

This journal is © the Owner Societies 2026

Phys. Chem. Chem. Phys., 2026, **28**, 8618–8625 | **8625**